The GRP Treatment of 2-D Complex Wave Structures

M. Ben-Artzi and J. Falcovitz

Institute of Mathematics, Hebrew University of Jerusalem, Israel
mbartzi@math.huji.ac.il, *ccjf@math.huji.ac.il*

1 Introduction

Solutions to initial value problems of hyperbolic conservations laws often involve discontinuities satisfying appropriate jump conditions. In the case of fluid dynamics, the 1-D equations admit two types of discontinuous waves – a shock discontinuity and a contact discontinuity. When fluid dynamics in two space dimensions is considered, even for the simplified "Riemann-type" problems (where the data are piecewise constant in sectors of the plane), a surprisingly rich variety of wave structure may evolve. Generally speaking, exact solutions of such fluid dynamical wave structures are not available and one must resort to approximations, such as those obtained by the high-resolution GRP scheme for hyperbolic conservation laws.

Studies of the family of 2-D scalar (nonlinear) conservation laws with Riemann-type initial data, for example the so-called Guckenheimer equation (see [3], and [1]), have shown that the resulting wave structures appear similar to those obtained in the fluid dynamical case. For some particular initial data [1], the wave interaction gives rise to a quite complex wave structure that includes an oblique shock, a sonic shock, a triple point, and a centered rarefaction wave (CRW). Here an exact solution is available, so that the GRP finite-difference approximation can be validated by verifying that it correctly produces all features of the solution.

In the present paper we therefore concentrate on two sample problems, one being the (scalar) Guckenheimer equation, the other a fluid dynamical interaction of a centered rarefaction wave with a converging nozzle. In both cases we present the GRP finite-difference solution. However, whereas in the scalar case it is compared to the exact solution, in the fluid dynamical case we compare it to the corresponding quasi-one-dimensional approximation – with interesting conclusions regarding this simplified approximation.

The GRP conservation law scheme is based on a solution (at each cell interface) of a "generalized Riemann problem", which is the initial value problem with piecewise linear data. Fluxes obtained this way lead to a second-order accurate, "high-resolution" integration of the conservation law. The analytic solution of the GRP at cell-boundaries is used not only for the evaluation of numerical fluxes but also, independently, for the evaluation of the

new slopes. Thus, the slopes are updated by using the underlying differential equations, rather than resorting to a "reconstruction" procedure. This proves to be an important feature of the GRP-scheme, which distinguishes it from practically all other existing "high-resolution" schemes. Indeed, the GRP-scheme used here can be viewed as a predecessor to the emerging "discontinuous Galerkin" scheme, which emphasize the use of "higher-order" approximations in computational cells, based on an analytic treatment of the differential equations.

In two space dimensions, we use a Strang-type operator splitting, employing the (1-D) GRP as the one-dimensional integration operator. We refer to the recent monograph [1] for a detailed description of the GRP scheme. We point out the fact that while the split scheme is formally second-order, it is not at all clear that, in complex wave-patterns, it retains the same quality of resolution as achieved in 1-D calculations. This aspect of the approximation is also examined in this paper, using the exact (in the scalar case) solution.

The plan of this article is to start with a description of the Guckenheimer problem and its exact solution. We then present the GRP solution to this problem, and compare it to the exact solution. This is followed by a problem of fluid dynamical wave interaction, where two types of (GRP) finite-difference solutions are considered – the quasi-one-dimensional approximation, and the full 2-D solution.

2 The Guckenheimer Equation

We consider the initial value problem (IVP) for the equation,

$$u_t + f(u)_x + g(u)_y = 0, \tag{1}$$

$$u(x, y, 0) = \phi(x, y), \quad (x, y) \in \mathbb{R}^2, \tag{2}$$

where $u(x, y, t)$ is a real (scalar) function and $f(u)$, $g(u)$ are real smooth flux functions. In the "Guckenheimer equation" $f(u) = \frac{1}{2}u^2$ and $g(u) = \frac{1}{3}u^3$.

A "Riemann type" problem for (1) is the IVP where $\phi(x, y)$ is finitely valued and homogeneous of order zero,

$$\phi(x, y) = u_0(\theta), \quad \theta = \arg(x, y) \quad (= \arctan \frac{y}{x}), \tag{3}$$

Here we take the initial data

$$u_0(\theta) = \begin{cases} 0, & 0 < \theta < \frac{3\pi}{4}, \\ 1, & \frac{3\pi}{4} < \theta < \frac{3\pi}{2}, \\ -1, & \frac{3\pi}{2} < \pi < 2\pi. \end{cases} \tag{4}$$

The solution is self-similar, i.e., it is a function of the two variables $\xi = x/t$, $\eta = y/t$. Referring to the wave structure of the exact solution shown in

Figure 1, we notice that outside of a large disk it consists of the following three shocks:

(a) A shock emanating (initially) from the line ($y = 0,\ x > 0$), moving at speed $1/3$ in the positive y direction (note that $g(u) = u^3/3$ is concave on $[-1, 0]$).
(b) A standing shock along the line ($x = 0,\ y < 0$).
(c) A shock emanating (initially) from the line ($x + y = 0,\ x < 0$). The self-similar analysis shows that at $t > 0$ this line is given by $x + y = (5/6)t$.

The interaction of these three shocks in a disk around $(0, 0)$ gives rise to a very complex wave structure. At time $t = 1$ it can be described as follows (see Figure 1(b)). The shock **(b)** extends to a segment of the positive y-axis $0 \le y \le b,\ b = 0.2823057$. At the point $(0, b)$ it bifurcates into a CRW whose tail characteristic is a sonic shock, across which the solution $u(x, y, 1)$ jumps from -1 to the value $\tilde{v} = 0.6087418$. Then u increases across the rarefaction from $\tilde{v}$ to 1, and it is constant along each (straight) characteristic line. The rarefaction wave modifies shock **(c)** causing its front to curve. Note that the head characteristic of the CRW carries the value $u = 1$. It intersects the shock **(c)** at the point (x_0, y_0) given by

$$x_0 = \frac{\frac{5}{6} - b}{2 - b}, \qquad y_0 = \frac{\frac{5}{6} + \frac{b}{6}}{2 - b}. \tag{5}$$

The tail characteristic (sonic shock) intersects the shock **(a)** at the point $(\tilde{\xi}, \frac{1}{3})$, where $\tilde{\xi} = 0.3519610$. The result of the interaction between the CRW and the shock **(c)** leads, as noted above, to a "bending" of the latter, forming a shock branch $y = y(x)$ connecting (x_0, y_0) to $(\tilde{\xi}, \frac{1}{3})$. It can be determined by solving an ordinary differential equation (see [2]). Thus, we obtain a wave pattern that includes a shock wave bifurcating into a CRW and a sonic shock which serves as a tail characteristic of the CRW. It intersects with the other two shocks at the triple point $(\tilde{\xi}, \frac{1}{3})$. This wave pattern provides for a good test of finite-difference schemes.

Two numerical tests were performed, one using the Godunov scheme and the other with the GRP scheme. The computation domain was the square $[-1 \le x \le 1,\ -1 \le y \le 1]$ which was divided into 320×320 square cells. The time step was $\Delta t = 0.003125$ (i.e., $\mu_{CFL} = 0.5$ since $max|u| = 1$ and $f'(u) = u,\ g'(u) = u^2$), and the computation was performed to final time $t = 1$. The boundary conditions were specified by calculating the exact solution on the outer segments of boundary cells. This is possible as long as the domain boundary is intersected only by the three shocks **(a), (b), (c)**, which according to Figure 1(b) is still true at $t = 1$.

The results are shown in the sub-domain $[-0.05 \le x \le 0.60,\ 0 \le y \le 0.65]$ [see Figure 2(a) for the Godunov scheme, and Figure 2(b) for the GRP scheme]. Recall that inside the rarefaction fan u is constant along the (straight) characteristic lines, so that numerical U-level curves approximate

the fan structure. The U-level sequence (6) given below is designed to show the shock fronts and the rarefaction fan. The five levels $L = 9, ..., 13$ correspond to the tail, head and three inner characteristic lines of the rarefaction fan [as shown in Figure 1(b)].

$$U_L = \begin{cases} -1 + 0.2\,L & \dots \quad L = 0, 1, ..., 8 \\ 0.60874,\ 0.68295,\ 0.76366,\ 0.86089,\ 1, & \dots \quad L = 9, ..., 13. \end{cases} \tag{6}$$

In order to enable interpolation at the lowest and highest U-levels, they were slightly shifted to -0.990 and 0.997, respectively. For comparison of the exact and numerical solutions, we represent the exact solution [Figure 1(b)] by discrete "marker points" situated on shock fronts, as shown in Figure 2. Additional marker points are located at points (x, y) inside the rarefaction fan, where the exact solution takes on the values U_L, $L = 9, ..., 13$ given by (6).

Our primary observation with respect to the numerical solution is that both finite-difference schemes (applied by Strang-type operator splitting) produce a correct approximation to this complex 2-D wave-interaction pattern [Figure 2]. The GRP solution agrees quite well with the exact one, whereas the Godunov solution shows a nearly equal agreement for the shock fronts, but a lesser agreement in the rarefaction fan. In this centered fan, the characteristic line that coincides with the sonic shock front corresponds to a constant value of $u = \tilde{v}$, and it is one of the U-level lines plotted ($L = 9$). In the GRP solution this line is seen very near the sonic shock front (Figure 2(b)), whereas in the Godunov case its stand-off distance is perceptibly higher [Figure 2(a)]. The captured sonic shock is represented by the cluster of level lines $L = 0, ..., 9$ (since the jump across this shock is from $u = U_0$ to $u = U_9$). At the other end of the rarefaction fan, the head characteristic line is plotted with $U_{13} = 0.997$ (close to the exact value of $U_{13} = 1$, for a clear U-level interpolation). In the Godunov solution this line extends well beyond the exact solution, whereas in the GRP solution it agrees well with the exact marker points. The rarefaction fan is the only region of the solution where $u(x, y, 1)$ varies smoothly with a non-zero gradient. Hence, these observations indicate that in such regions the (second-order accurate) GRP scheme produces considerably smaller errors than the (first-order accurate) Godunov scheme. In what concerns the bifurcation point $(0, b)$ and the triple point $(\tilde{\xi}, \frac{1}{3})$, resulting from the two-dimensional setting, we observe that they are well replicated by both schemes.

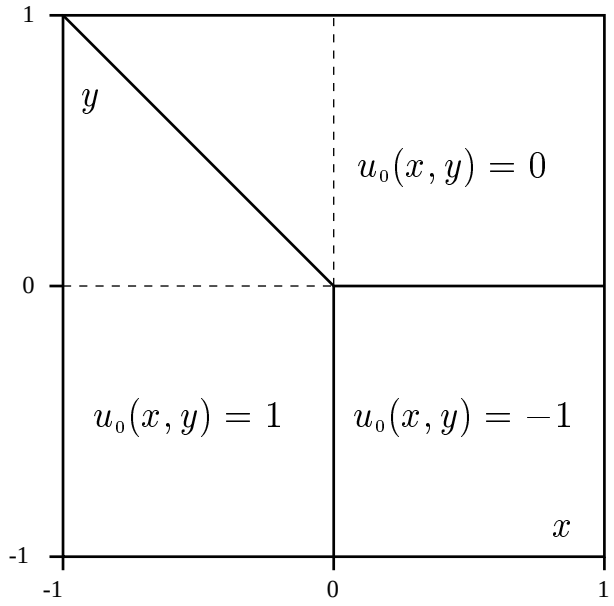

(a) Initial data for Guckenheimer Structure

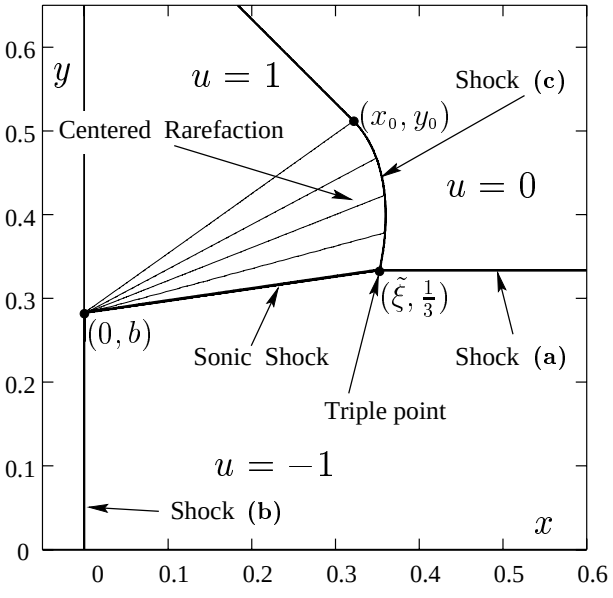

(b) Exact Guckenheimer Structure at $t = 1$

Fig. 1. The Guckenheimer Structure for $u_t + (u^2/2)_x + (u^3/3)_y = 0$.

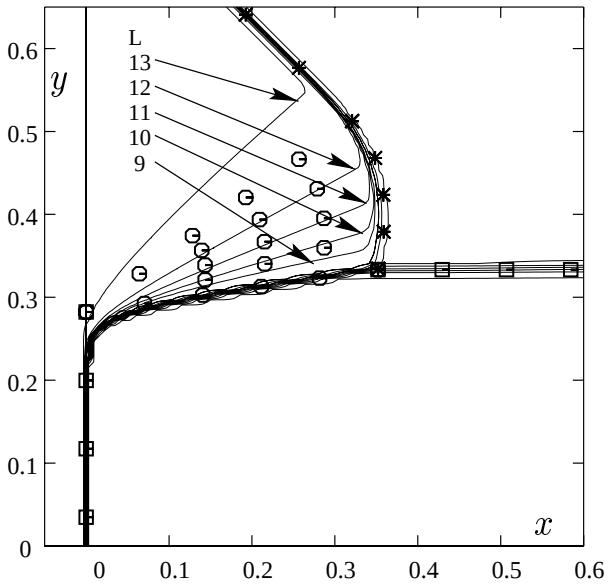

(a) First-order (Godunov $\Delta x = \Delta y = 0.00625$)

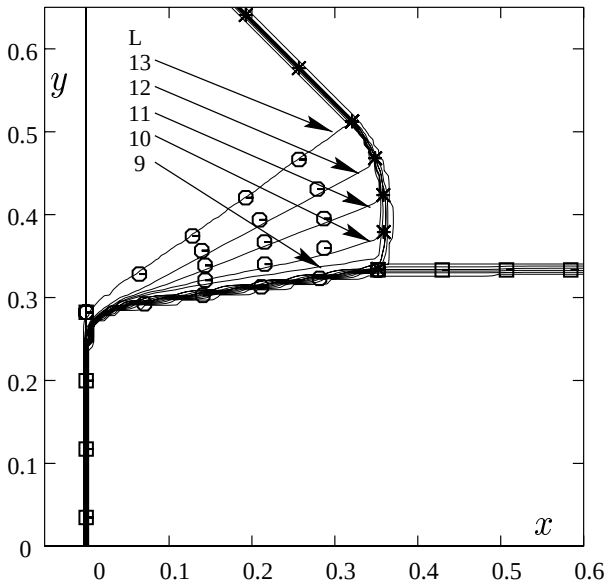

(b) Second-order (GRP $\Delta x = \Delta y = 0.00625$)

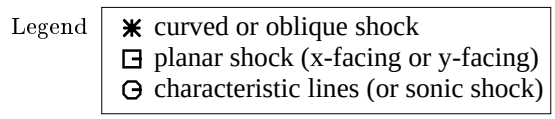

Fig. 2. U-level curves for Guckenheimer equation at $t = 1$
$u_t + (u^2/2)_x + (u^3/3)_y = 0$. Initial data in Figure 1(a).

3 Interaction of a Centered Rarefaction Wave with a Converging Nozzle

Consider a centered rarefaction wave that propagates in a planar duct comprising two long segments of uniform cross-section area joined by a smooth converging nozzle. Such processes take place in numerous systems of industrial and scientific interest. The significance of this sample flow lies in the comparison we make between a full multidimensional solution and the corresponding quasi-1-D approximation. The reason is that the latter (often referred to as the "duct flow" approximation) is commonly employed as an engineering design tool. Hence, studying the bounds of its validity as a simplified approximation to the full multidimensional solution is highly significant to engineering design and analysis.

For the multidimensional computation of the wave interaction with a converging nozzle we employ the operator-split 2-D GRP scheme where the symmetric duct contour intersects an underlying two-dimensional Cartesian grid, using the "moving boundary" scheme (where the boundary is stationary). We refer to [1] for details of the MBT scheme and the nozzle contour, as well as to a more comprehensive analysis of the present wave interaction problem.

We consider the case of a 1:10 pressure ratio centered rarefaction wave (CRW) in a fluid assumed to be a perfect gas with $\gamma = 1.4$. The CRW is initially located in the wider part of the duct, and it propagates towards a (short) converging nozzle of $2:1$ cross-section area ratio. The initial data is that of a Riemann problem designed to produce a right-facing CRW. It consists of two uniform states $\mathbf{U}_L=[\rho_L, p_L, u_L]=[0.27030, 0.1, -1.4016]$, $x < 1.3$, and $\mathbf{U}_R=[\rho_R, p_R, u_R]=[1.4, 1, 0]$, $x > 1.3$. The location of the initial discontinuity ($x = 1.3$) is just ahead of the converging segment that occupies the interval $1.6 \leq x \leq 2.6$ (see Figure 3 at $T = 0$).

The 2-D computation is conducted in the (symmetric) upper half of the duct, embedding it in the rectangular domain $(x, y) \in [-1.6, 9.4] \times [0, 1]$, which is divided into a grid of 550×50 square cells ($\Delta x = \Delta y = 0.02$). A rigid-wall boundary condition (due to symmetry) is imposed at the nozzle contour and at the centerline ($y = 0$). On the left and right sides of the computational rectangle we impose "non-reflecting" boundary conditions, designed to allow waves to pass through these endplanes (almost) undisturbed. The computation was performed in the time interval $[0, 9]$, with time steps adjusted (at each integration cycle) to have a nearly constant CFL coefficient $\mu_{CFL} = 0.7$.

The quasi-1-D computation was conducted in the same x interval, with the same spatial grid, the same contour area function $A(x)$, and the same inflow/outflow boundary conditions as in the 2-D case. The computation was performed with time steps adjusted to have the same $\mu_{CFL} = 0.7$ and in the same time interval $[0, 9]$.

The results of the 2-D computation are shown as a time-sequence maps of isobars ($p = const.$) in Figure 3. Notice that in the initial state $\mathbf{U}_L$ the flow is

already supersonic since $u_L = -1.947 c_L$, so that $|u_L| > c_L$. Thus, a supersonic expansion flow gradually evolves in the *diverging* direction of the nozzle.

From the time-sequence of isobars plots (Figure 3), we observe that the flow over-expands in the nozzle, so that an upstream-facing oblique shock wave is formed (marked by $*$ in Figure 3). It serves to align the flow velocity vector with the (straight) duct contour, and to match the pressure to that prevailing further left in the wider duct segment. Another complex shock interaction forms at the centerline ($y = 0$), and evolves into a full Mach reflection.

In Figure 4 we compare the results of the 2-D and quasi-1-D computations at the final time $t = 9$, showing an isobars map (as in the last frame of Figure 3), followed by profiles of density, pressure, and flow Mach number, as functions of the centerline coordinate (Figures 3(b)–(d)).

The two solutions are in close agreement throughout the narrower duct segment ($x > 2.6$), but disagree elsewhere. At the entrance to the nozzle ($x = 2.6$), the flow speed is sonic ($M = 1$ in 4(d)), enabling the nozzle flow to approach a *steady* supersonic expansion flow, commencing at a virtual sonic plane ("nozzle entrance"), which serves to "match" the *unsteady* rarefaction wave on its right to the steady flow on its left. In other words, upon passing through the nozzle, the CRW is "split" into a "transmitted" part and a "reflected" part, the two being separated by a (nearly) steady flow through the diverging nozzle.

Now the source of disagreement between the quasi-1-D and the 2-D solutions is evident. The fluid expands as it (reversely) flows through the nozzle at supersonic speed, and a full 2-D description of this flow involves an oblique shock system at the nozzle exit (Figure 4(a)), which is poorly approximated by the cross-section-averaged quasi-1-D solution that relies on a normal shock for matching the over-expanded supersonic nozzle flow to the pressure ahead. Moreover, the flow passing through the Mach reflection shock structure is separated by the slip-line into two streams having distinctly different thermodynamic properties. Naturally, the 1-D "averaging" of these two streams involves significant deviations from the 2-D flow field.

It is concluded that although quasi-1-D calculations may generally be adequate as an engineering approximation, a verification by comparison to the appropriate multidimensional solution is required in order to make sure that the disagreement between the two remains within acceptable bounds. Our test case analysis thus brings out the significance of full multidimensional numerical solutions; the (simpler) quasi-1-D solutions may not always serve as adequate approximations.

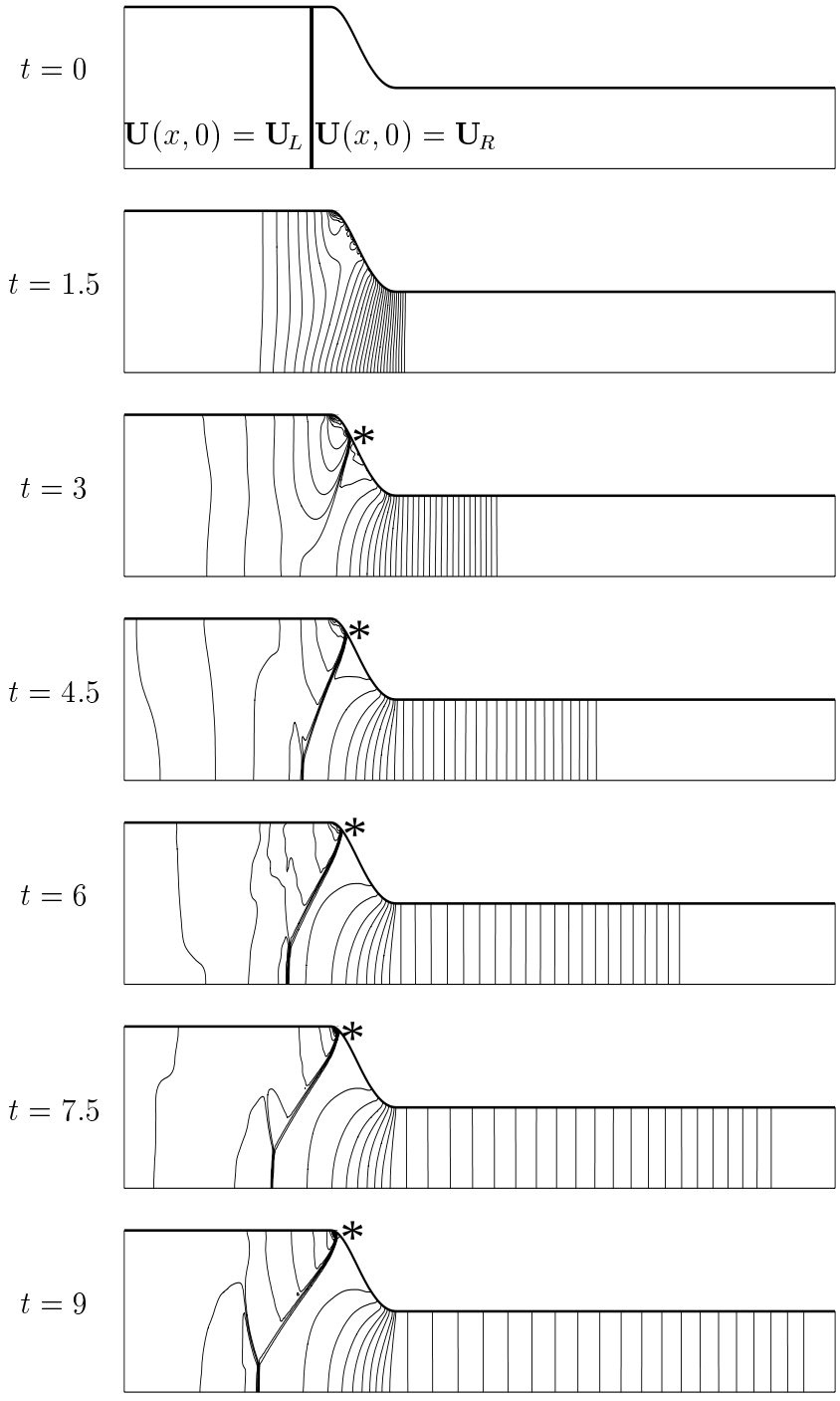

Fig. 3. Time sequence of CRW interaction with a converging segment.
Isobars map. The * marks shock formation at duct wall.
(Duct width here is twice the true size, for better visibility).

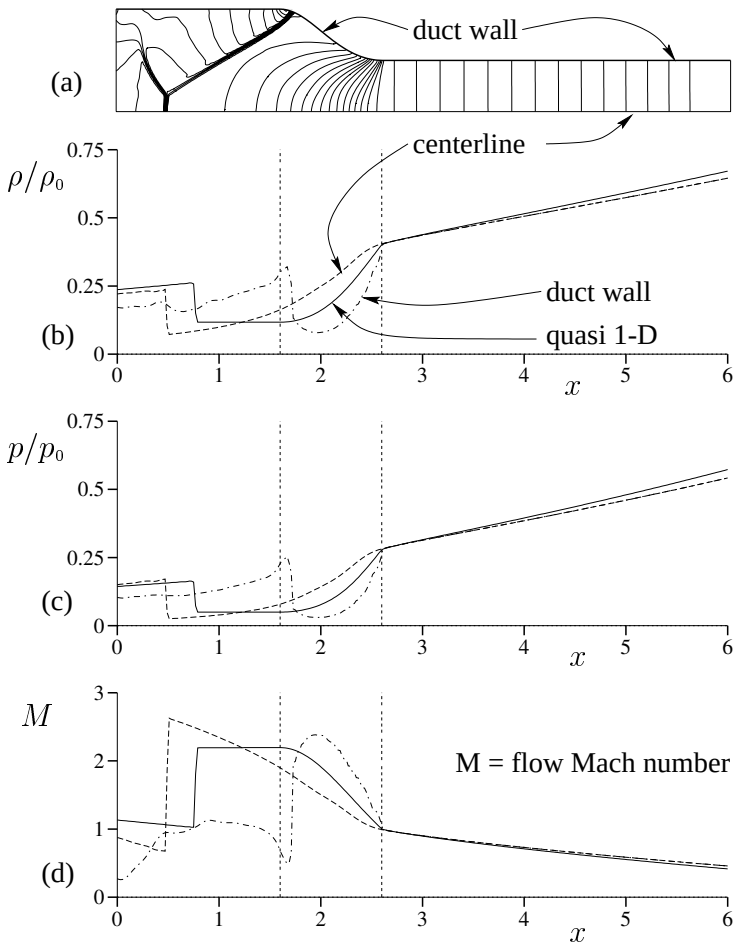

Fig. 4. CRW interaction with a converging segment; comparison of 2-D and quasi-1-D results at time $t = 9$.
(a) Isobars of 2-D calculation.
(b)–(d) Quasi 1-D solution. Distribution of density, pressure and flow Mach number (taken as positive).

References

1. M. Ben-Artzi and J. Falcovitz (2002): Generalized Riemann Problems in Computational Fluid Dynamics. Cambridge University Press, London, New York (in press).
2. M. Ben-Artzi, J. Falcovitz, and J. Li (2001): Wave interactions and numerical approximations for two-dimensional scalar conservation laws. Preprint, Institute of Mathematics, Hebrew University of Jerusalem.
3. J. Guckenheimer (1975): Shocks and rarefactions in two space dimensions. Arch. Rational Mech. Anal., **59**, 281–291.